Vortices in rotating systems: Centrifugal, elliptic and hyperbolic type instabilities

D. Sipp, E. Lauga, and L. Jacquin
ONERA, 29 avenue de la Division Leclerc, BP 72, F-92322 Chatillon Cedex, France

(Received 11 June 1999; accepted 18 August 1999)

This paper is devoted to the effects of rotation on the linear dynamics of two-dimensional vortices. The asymmetric behavior of cyclones and anticyclones, a basic problem with respect to the dynamics of rotating flows, is particularly addressed. This problem is investigated by means of linear stability analyses of flattened Taylor–Green vortices in a rotating system. This flow constitutes an infinite array of contra-rotating one-signed nonaxisymmetric vorticity structures. We address the stability of this flow with respect to three-dimensional short-wave perturbations via both the geometrical optics method and via a classical normal mode analysis, based on a matrix eigenvalue method. From a physical point of view, we show that vortices are affected by elliptic, hyperbolic and centrifugal instabilities. A complete picture of the short-wave stability properties of the flow is given for various levels of the background rotation. For Taylor–Green cells with aspect ratio $E=2$, we show that anticyclones undergo centrifugal instability if the Rossby number verifies $\mathrm{Ro}>1$, elliptic instability for all values of Ro except $0.75<\mathrm{Ro}<1.25$ and hyperbolic instability. The Rossby number is here defined as the ratio of the maximum amplitude of vorticity to twice the background rotation. On the other hand, cyclones bear elliptic and hyperbolic instabilities whatever the Rossby number. Besides, depending on the Rossby number, rotation can either strengthen (anticyclonic vortices) or weaken elliptic instability. From a technical point of view, in this article we bring an assessment of the links between the short-wave asymptotics and the normal mode analysis. Normal modes are exhibited which are in complete agreement with the short-wave asymptotics both with respect to the amplification rate and with respect to the structure of the eigenmode. For example, we show centrifugal eigenmodes which are localized in the vicinity of closed streamlines in the anticyclones; elliptical eigenmodes which are concentrated in the center of the cyclones or anticyclones; hyperbolic eigenmodes which are localized in the neighborhood of closed streamlines in cyclones. © *1999 American Institute of Physics.* [S1070-6631(99)00912-5]

I. INTRODUCTION

Rotation strongly affects the evolution and properties of three-dimensional turbulence. In a rotating tank, Hopfinger, Browand and Gagne[1] observe the rapid formation of coherent structures, which are quasi two-dimensional vortices aligned with the rotation axis. These structures, which do not emerge in the nonrotating case, comprise intense cyclonic vortices and (much) weaker anticyclonic vortices. The experiments of Kloosterziel and van Heijst[2] also showed a strong asymmetry in behavior between released cyclones and anticyclones: the cyclones remain two-dimensional at all times whereas anticyclones are first disrupted into 3D turbulence and 2D columnar structures then re-emerge after some time. The Rayleigh centrifugal instability,[2,3] which is a three-dimensional mechanism, is responsible for these phenomena. The dynamics of such an instability may be captured by a model based on a single-signed vorticity structure, as, for example, in the numerical simulations by Carnevale *et al.*[4] A 2D barotropic instability[5,6] which is governed by Rayleigh's ''inflection point'' criterion may also develop in an isolated vortex which has zero net circulation (multiple-signed vorticity structures). This 2D mechanism of instability does not differentiate cyclones and anticyclones which both can undergo barotropic instability. In experiments, this barotropic instability is only observed in cyclones where multipoles are generated, anticyclones being dominated by the 3D centrifugal instability described above (see Orlandi and Carnevale[7]).

In the present paper we focus on the link between linear stability and the asymmetric behavior between cyclones and anticyclones. Fully 3D perturbations have therefore to be considered. In this article, we will focus on short-wave perturbations. These short-wave instabilities are analyzed in a rotating Taylor–Green flow which is an array of contra-rotating single-signed vortices. Two different techniques are used: the geometrical optics method and a normal mode analysis. In the geometrical optics method introduced by Eckhoff[8] and Lifschitz and Hameiri,[9] a localized short-wave perturbation is characterized by a wavevector $\mathbf{k}$ and an amplitude vector $\mathbf{a}$, that we follow along the particle trajectories of the flow. The flow is unstable if there exists a streamline on which a particular solution $\mathbf{a}(t)$ grows unboundedly as $t\to\infty$. The classical normal mode analysis considers normal modes of the form $(\mathbf{u}',p')=(\tilde{\mathbf{u}},\tilde{p})\exp(ikz)\exp(st)$ where k is the vertical wavenumber and s the complex amplification rate, the flow lying in the (x,y) plane orthogonal to the rotation axis. The flow is unstable if a normal mode exhibits a complex amplification rate s which has a positive real part.

Note that the eigenmode $(\tilde{\mathbf{u}},\tilde{p})$ has to be square integrable, otherwise it belongs to the continuous spectrum.

Physically, the short-wave instabilities can be explained by local vorticity stretching. Three different types of short-wave instabilities exist, the elliptic, hyperbolic and centrifugal ones, depending on the stretching directions. Elliptic instability[9–13] occurs on elliptically shaped streamlines and hyperbolic instability[9,14–18] takes place at hyperbolic stagnation points. The extension to rotating systems has been done in Refs. 19–22 for elliptic instabilities and in Refs. 22–24 for hyperbolic instabilities. Differentiation between cyclones and anticyclones appears for elliptic instability but not for hyperbolic instability if the hyperbolic points are irrotational (which is the case with the Taylor–Green flow). Centrifugal short-wave instabilities were first identified by Bayly[25] who generalized the classical Rayleigh centrifugal instability criterion to general nonaxisymmetric plane flows. The extension to the rotating case has been achieved in Ref. 26.

In this article, we consider the Taylor–Green vortices in a rotating frame and characterize its short-wave stability properties for various levels of background rotation. This will enable us to differentiate the dynamics of cyclones and anticyclones through the determination of the stable and unstable regions in the parameter space. The choice of the Taylor–Green flow will also enable us to assess the impact of the nonaxisymmetry of the vortices. It should be noted that nearly all stability studies in the present field are constraint to circular vortices. Hence, elliptic and hyperbolic type instabilities, which are intrinsically nonaxisymmetric, are always left aside and only circular centrifugal type instabilities are usually considered. Secondly, an important question concerns the link between the short-wave asymptotics and the normal mode analysis. In this article we aim at giving a further assessment of this link. Partial results exist on this point. In a specific case, Bayly[25] explained how the short-wave asymptotics formalism could be used to construct localized amplified normal modes. Direct comparisons between linearized direct numerical simulation results and short-wave asymptotics' results have also shown[27] a qualitative agreement between the two approaches. Qualitative and quantitative agreement has been obtained[28] for elliptic instability occurring in the center of flattened Taylor–Green vortices. But a general theory making the link between the short-wave asymptotics and a normal mode analysis is still lacking.[29,30] The paper is organized as follows. After a brief description of the Taylor–Green flow, Sec. III is devoted to the short-wave asymptotics which will give a complete picture of the short-wave stability properties of both cyclonic and anticyclonic vortices. These results are then compared to a normal mode analysis in Sec. IV. There, we try to make a general assessment on the link between the short-wave asymptotics and a normal mode analysis.

II. THE TAYLOR–GREEN FLOW

We consider the Taylor–Green flow which is characterized by the x and y periodicities $2\pi a$ and $2\pi b$ and the maximum vorticity $W>0$ (see Fig. 1). The corresponding streamfunction is

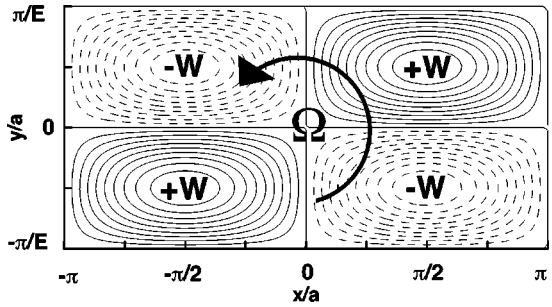

FIG. 1. The Taylor–Green flow: iso-values of the vorticity ζ. This stationary basic flow forms a 2D array of contra-rotating vortices. The magnitude of the vorticity in the center of the vortices is W, the periodicities in the x and y directions are $2\pi a$ and $2\pi b$, respectively, and the background rotation is Ω. $E=a/b$ is the aspect ratio. Case $E=2$.

$$\psi(x,y)=\frac{W}{1/a^2+1/b^2}\sin\frac{x}{a}\sin\frac{y}{b}. \tag{1}$$

This is an exact solution of the inviscid Euler equations in a frame rotating at the angular velocity Ω, which will be considered as positive. The dimensionless parameters are the following: the aspect ratio $E=a/b$, the Reynolds Number $\mathrm{Re}=a^2W/\nu$ and the Rossby number $\mathrm{Ro}=W/2\Omega$. In the following, we take $L=a$ and $T=W^{-1}$ as unit length and time scales. The nondimensional streamfunction is thus given by $\psi=(\sin x\sin Ey)/(1+E^2)$ and the nondimensional linearized Navier–Stokes equations read as

$$\frac{\partial\mathbf{u}'}{\partial t}+\mathbf{u}'\cdot\nabla\mathbf{u}+\mathbf{u}\cdot\nabla\mathbf{u}'=-\nabla p'-\frac{1}{\mathrm{Ro}}\mathbf{e}_z\times\mathbf{u}'+\frac{1}{\mathrm{Re}}\Delta\mathbf{u}', \tag{2}$$

$$\nabla\cdot\mathbf{u}'=0, \tag{3}$$

where $\mathbf{u}$ is the 2D basic flow related to the above streamfunction ψ and $(\mathbf{u}',p')$ are the 3D perturbations.

III. THE SHORT-WAVE ASYMPTOTICS

A. Presentation

In this section, we study the short-wave stability properties of the steady Taylor–Green flow $\mathbf{u}(\mathbf{x})$. Following Lifschitz and Hameiri,[9] we consider a rapidly oscillating localized perturbation subject to rotation 1/Ro evolving along the trajectory $\mathbf{x}(t)$ and characterized by a wavevector $\mathbf{k}(t)$ and a velocity envelope $\mathbf{a}(t)$. These quantities are governed by the following set of ordinary differential equations, which evolve along particle trajectories:

$$\frac{d\mathbf{x}}{dt}=\mathbf{u}(\mathbf{x}), \tag{4}$$

$$\frac{d\mathbf{k}}{dt}=-\mathcal{L}^T(\mathbf{x})\mathbf{k}, \tag{5}$$

$$\frac{d\mathbf{a}}{dt}=\left(\frac{2\mathbf{k}\mathbf{k}^T}{|\mathbf{k}|^2}-\mathcal{I}\right)\mathcal{L}(\mathbf{x})\mathbf{a}+\frac{1}{\mathrm{Ro}}\left(\frac{\mathbf{k}\mathbf{k}^T}{|\mathbf{k}|^2}-\mathcal{I}\right)\mathbf{e}_z\times\mathbf{a}, \tag{6}$$

where $\mathcal{L}=\nabla\mathbf{u}$ designates the velocity gradient tensor of the basic flow, $\mathcal{I}$ the identity tensor and the superscript T the

transpose. Lifschitz and Hameiri[9] proved that a sufficient criterion for instability is that this system has at least one solution for which the amplitude $\mathbf{a}(t)$ increases unboundedly as $t\to\infty$.

We restrict our analysis to the streamlines belonging to the two cells ($-\pi\leqslant x\leqslant 0$, $0\leqslant y\leqslant \pi/E$) and ($0\leqslant x\leqslant \pi$, $0\leqslant y\leqslant \pi/E$). As the problem is symmetric with respect to the transformation $x\to -x$, $y\to -y$ and $z\to z$, it is then easy to deduce the results for the two other cells ($-\pi\leqslant x\leqslant 0$, $-\pi/E\leqslant y\leqslant 0$) and ($0\leqslant x\leqslant \pi$, $-\pi/E\leqslant y\leqslant 0$). All streamlines are closed except those bounding the cells. Each closed streamline will be referred to in the following by its streamfunction value ψ and the corresponding time-period is noted $T(\psi)$. The maximum value of $|\psi|$, $\psi_m=1/(1+E^2)$, is reached in the center of the vortices. Let us introduce $\tilde{\psi}=\psi/\psi_m$. With Ro>0, the streamline $\tilde{\psi}=-1$ corresponds to the center of the anticyclonic vortex (left cell) whereas $\tilde{\psi}=+1$ refers to the center of the cyclonic vortex (right cell). $\tilde{\psi}=0$ denotes the cell-bounding streamlines.

In the case of closed streamlines, the differential equations (5) and (6) may be investigated by means of a Floquet theory by integrating the equations over one period. The origin of the streamline $\tilde{\psi}$ is defined by $\mathbf{x}(t=0)=[\arcsin\tilde{\psi},\pi/(2E)]$. It is sufficient to consider the case $\mathbf{k}(t=0)\cdot\mathbf{e}_y=0$ since[28] the other perturbations die out because of viscosity. Furthermore, the differential equation (6) for $\mathbf{a}(t)$ is independent of the wavenumber $|\mathbf{k}|$. Therefore results only depend on the co-latitude angle θ of the initial wavevector $\mathbf{k}(t=0)=\sin(\theta)\mathbf{e}_x+\cos(\theta)\mathbf{e}_z$. The stability properties of the streamline $\tilde{\psi}$ are then characterized by the 3 eigenvalues of the fundamental Floquet matrix associated to Eq. (6). It can be shown that one of them is 1 and that the other two must multiply to 1. Hence, the associated Floquet exponents, which are the natural logarithms of these eigenvalues divided by the turnaround $T(\psi)$, are s_1, s_2 and $s_3=0$ with the following properties: in the case of instability, $s_1=\sigma$, $s_2=-\sigma$ with $\sigma>0$; in the case of stability, $s_1=i\omega$, $s_2=-i\omega$ with $\omega>0$.

Finally, the co-latitude angle θ of the wave-vector at $t=0$ is taken in the interval $[0,\pi/2]$ since the Floquet exponents are invariant with respect to the transformations $\theta\to-\theta$ and $\theta\to\pi-\theta$. Given a streamline $\tilde{\psi}$ and a co-latitude angle θ, we now determine the numerical value of the real part of the Floquet exponent $\sigma(\tilde{\psi},\theta)$. The stability properties of the rapidly oscillating localized perturbations will therefore be characterized.

B. Results

Numerical results of the short-wave analysis are obtained by integrating numerically the equations (4), (5) and (6) by means of a classical fourth-order Runge–Kutta scheme. The results concerning the case $E=2$ are given in Fig. 2 for various values of the Rossby number: Ro $=0.4,1.25,2,4,7,25,100,10000$. For each Rossby number, we have sketched in the $(\tilde{\psi},\theta)$ plane the iso-values of the amplification rate $\sigma(\tilde{\psi},\theta)$. Each plot gives an exhaustive picture of the short-wave stability properties of the Taylor–Green flow, since the streamlines $-1\leqslant\tilde{\psi}<0$ correspond to the anticyclonic vortex and the streamlines $0<\tilde{\psi}\leqslant 1$ refer to the cyclonic vortex.

For weak background rotations Ro$=10000$, the plot is symmetric with respect to $\tilde{\psi}=0$. This means that anticyclones and cyclones behave similarly. But as the Rossby number decreases, this symmetry is broken so that the linear dynamics of anticyclones and cyclones differ.

The three different kinds of short-wave instabilities are present (elliptic, hyperbolic and centrifugal instabilities).

1. The elliptic instability

In the case Ro$=10000$, the cyclones and the anticyclones bear the well-known elliptic instability.[11,13,19,20] This instability is related to the elliptic shape of the streamlines in the center of the vortices. Only the perturbations with θ comprised in a given interval around $\theta=0.9$ are unstable. This case has been thoroughly investigated in Ref. 28.

When Ro decreases, we can follow the elliptic unstable regions in each cell:

(i) in the cyclonic vortices, the elliptic instability weakens as the background rotation increases: the unstable θ interval shrinks and the instability affects perturbations with increasing values of the co-latitude angle θ. Nevertheless, this instability never vanishes and cyclonic vortices are always elliptically unstable whatever the Rossby number;

(ii) in the anticyclonic vortices, the trend is opposite: as the Rossby number decreases, the unstable θ interval moves towards $\theta=0$ and the maximum value of the amplification rate σ, which is obtained for a given value of θ for the streamline $\tilde{\psi}=-1$, first increases to the value 0.3 obtained for Ro$=2$, then decreases down to zero for Ro$=1.25$. Below this Rossby number, the elliptic instability does not affect anymore the anticyclonic vortex until Ro$=0.75$. The flow then becomes elliptically unstable again (see the case Ro$=0.4$).

These features are summarized in Fig. 3. In the upper plot, we have sketched the maximum value of σ, which is obtained in the center of the vortices $\tilde{\psi}=\pm 1$, versus the Rossby number. In the lower plot, we have figured the corresponding θ angle where the above maximum occurs. Hence, as the Rossby number decreases, elliptic instability is first strengthened in anticyclonic vortices; then it weakens before vanishing below Ro$=1.25$. At Ro$=0.75$, it reemerges and is maintained down to Ro$=0$ where $\sigma\to 0.074$. This is a striking feature[21,31] which is observed also in the cyclones where the background rotation only weakens the elliptic instability without killing it. Note that these results are in accordance with those of some previously published articles: the case Ro$=0$ has already been considered in steadily rotating Kirchhoff–Kida vortices[21] and the so-called ''spanwise'' perturbations ($\theta=0$) have been investigated in Ref. 24.

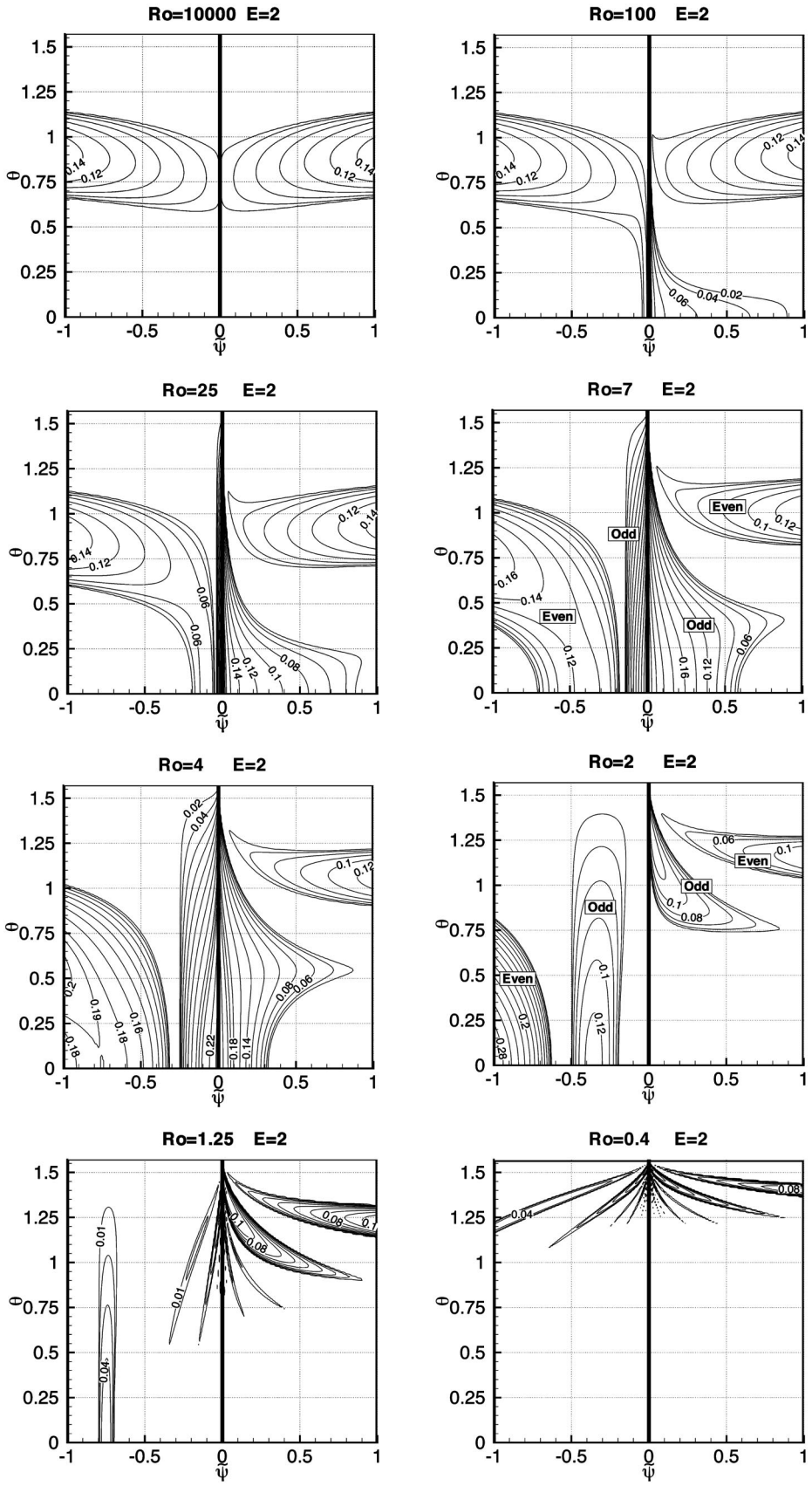

FIG. 2. Short-wave stability properties of the Taylor–Green flow for various Rossby numbers. Each plot sketches the iso-values of the real part of the Floquet exponent σ in the $(\tilde{\psi},\theta)$ plane. Case $E=2$.

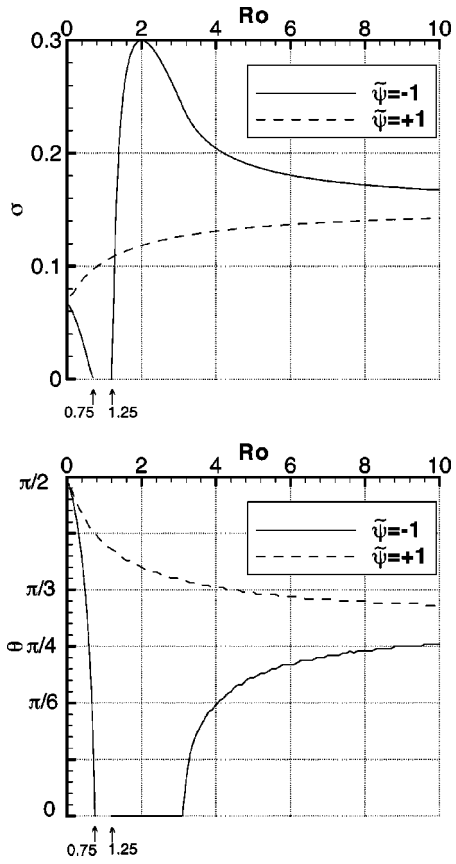

FIG. 3. Elliptic instability: short-wave stability results obtained in the center of the vortices $\tilde{\psi}=\pm 1$. The upper plot sketches the maximum amplification rate σ over the co-latitude angle θ versus the Rossby number. The lower plot figures the corresponding θ angle.

2. The centrifugal instability

The centrifugal instability only affects anticyclonic vortices. Weak anticyclones (Ro<1) are not affected by this instability. But, as Ro>1, an unstable $\tilde{\psi}$ interval appears (see the Ro=1.25 case) in the center of the anticyclonic vortex ($\tilde{\psi}=-1$) with maximum instability occurring for spanwise perturbations ($\theta=0$). As the Rossby number increases, the instability strengthens and moves out (see the Ro=2 case) towards the bounding streamline ($\tilde{\psi}=0$). One of the bounds of the unstable $\tilde{\psi}$ interval always corresponds to the streamline where the sign of the absolute vorticity $\zeta+2\Omega$ changes (ζ denotes the vorticity on the streamline $\tilde{\psi}$). This result is in accordance with Ref. 26 where it has been conjectured that a flow with closed streamlines is centrifugally unstable if the sign of the absolute vorticity changes somewhere in the flow. Physically, the centrifugally unstable streamlines $\tilde{\psi}$ are characterized by the negativity of the following quantity somewhere along $\tilde{\psi}$:

$$\delta(x,y)=2\left(\frac{V}{\mathcal{R}}+\Omega\right)(\zeta+2\Omega), \tag{7}$$

where V is the local norm of the velocity and $\mathcal{R}$ the local algebraic radius of curvature.[26] This is a local form of the axisymmetric criterion of instability given by Kloosterziel and van Heijst.[2]

3. The hyperbolic instability

The classical hyperbolic instability[9,17,22,24] is obtained at the hyperbolic stagnation points of the flow with spanwise perturbations ($\theta=0$). For $E=2$, the corresponding amplification rate is the following: $\sigma(\tilde{\psi}=0,\theta=0)=0.4\sqrt{1-(2.5/\mathrm{Ro})^2}$ if Ro>2.5. The flow is hyperbolically stable on the stagnation points for lower Rossby numbers.

In the case of weak background rotation (high Ro), only the streamline $\tilde{\psi}=0$ bears the hyperbolic instability.[28] But as Ro decreases, streamlines near $\tilde{\psi}=0$ become affected: this can be seen, for example, in the case Ro=7 where a large number of closed streamlines are hyperbolically unstable both in the cyclonic and in the anticyclonic vortices.

For Ro<2.5, spanwise perturbations are not unstable anymore on the hyperbolic stagnation points. But the vortices still exhibit unstable streamlines near $\tilde{\psi}=0$ but at high co-latitude angles θ.

IV. NORMAL MODE ANALYSIS

Thanks to the short-wave asymptotics, we have completely characterized the short-wave stability properties of the Taylor–Green flow. In this section, we make a thorough investigation of the correspondence between the short-wave asymptotics and a normal mode analysis by means of a matrix eigenvalue method. For the specific case of spanwise perturbations ($\theta=0$), Bayly showed explicitly how normal modes could be constructed from the short-wave asymptotics results. Section IV A is devoted to the results that can be obtained with this formalism. Other correspondences are addressed in Sec. IV B where the matrix eigenvalue method is developed. There, we will first try to retrieve the features obtained in Sec. IV A for spanwise perturbations, then try to make a further assessment on the link between the short-wave asymptotics and the normal mode analysis.

A. The spanwise centrifugal and elliptic instabilities in the anticyclonic vortex

In the specific case of spanwise perturbations ($\theta=0$), Bayly[25] explained how the short-wave asymptotics formalism could be used to construct localized amplified normal modes. As shown in Appendix A, if the short-wave amplification rate $\sigma(\psi)$ of the spanwise perturbations verifies $\sigma'(\psi_0)=0$ and $\sigma''(\psi_0)<0$ for some streamline ψ_0 then a family ($n=0,1,2,\ldots$) of normal modes localized in the neighborhood of the streamline ψ_0 could be constructed. The amplification rate s_n of each member n of this family behaves as $s_n=\sigma(\psi_0)-\mu_n/k$ with $\mu_n=(2n+1)\mu_0$ where μ_0 is a positive constant. Hence, a local maximum of $\sigma(\psi,\theta=0)$ near ψ_0 is related to an infinite set of localized eigenmodes near ψ_0. The amplification rates of all these eigenmodes converge towards the short-wave value $\sigma(\psi_0,\theta=0)$ as $k\to\infty$.

In this section, we apply this formalism and look for streamlines ψ_0 where $\sigma'(\psi_0)=0$ and $\sigma''(\psi_0)<0$. In Fig. 2, we can see that this happens in the anticyclonic vortex for the centrifugal instability (case Ro=2) and also for the spanwise elliptic instability (case Ro=7). We now vary the

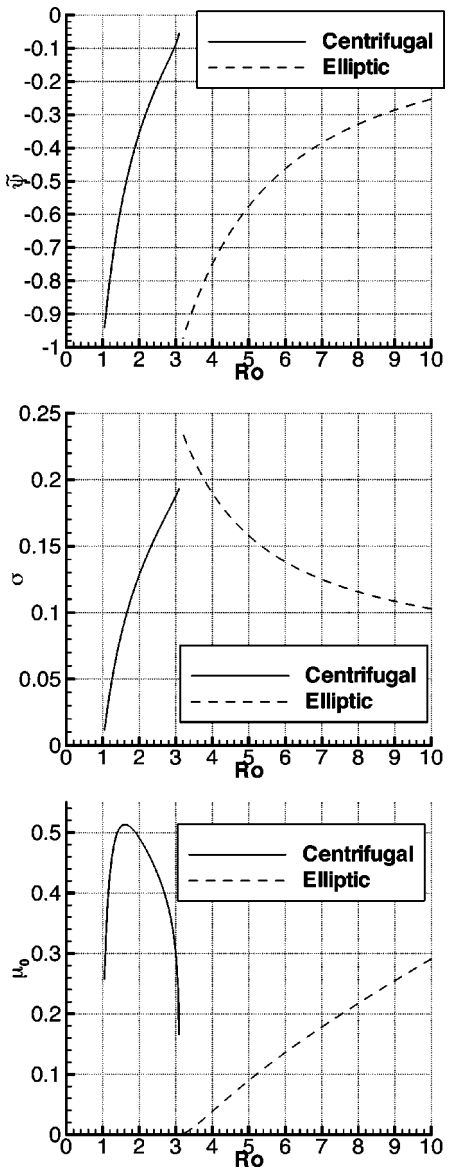

FIG. 4. Spanwise ($\theta=0$) centrifugal and elliptic instabilities in the anticyclonic vortex for various Rossby numbers. The upper plot gives the streamline $\tilde{\psi}$ in the neighborhood of which the eigenmode is constructed [$\sigma'(\tilde{\psi})=0$ and $\sigma''(\tilde{\psi})<0$]. Middle plot: corresponding amplification rate σ. Lower plot: eigenvalue convergence parameter μ_0 of the $n=0$ branch.

Rossby number and follow these streamlines. For each Rossby number we have sketched in Fig. 4, the location of these streamlines $\tilde{\psi}$, the corresponding amplification rate σ and the eigenvalue convergence parameter μ_0. The following conclusions can be drawn from these plots: if $1<\mathrm{Ro}<3.2$, we can explicitly construct centrifugal normal modes and if $\mathrm{Ro}>3.2$, we can build elliptic normal modes.

It can also be shown that the centrifugal normal modes are odd with respect to the center of the anticyclonic vortex and that the elliptic normal modes are even. This comes from the symmetry properties of the basic flow which induce analogous symmetries for the normal modes. These symmetries — even or odd — were depicted in Fig. 2 in the cases $\mathrm{Ro}=2$ and $\mathrm{Ro}=7$.

B. The matrix eigenvalue method

The technical presentation of the matrix eigenvalue method is given in Appendix B. For a given set of values of the aspect ratio E, the Rossby number Ro, the wavenumber k and the Reynolds number Re, a discrete spectrum of eigenvalues/eigenvectors is obtained. This discrete spectrum can be decomposed into four independent subsets referred by two parameters $\alpha=\pm1$ and $\beta=\pm1$. This decomposition comes from the fact that the eigenmodes are either even or odd both with respect to the center of the vortices and with respect to the origin.

The three basic short-wave instabilities (centrifugal, elliptic and hyperbolic ones) are now successively investigated by means of the matrix eigenvalue method. In each case, we show typical eigenmodes obtained for a given value of the wavenumber k. The precise convergence properties as $k\rightarrow\infty$ are postponed to Appendix C.

1. Centrifugal instabilities

Centrifugal instabilities are investigated for $\mathrm{Ro}=2$. The short-wave results were reported in Fig. 2. Figure 4 gives the characteristics of the normal modes deduced from Bayly's formalism. The Reynolds number is $\mathrm{Re}=\infty$ and the spatial resolution of the matrix eigenvalue method is: $-60\leqslant m,n\leqslant 60$. The spatial energy repartition of the most unstable centrifugal eigenmode of the $(\alpha=-1,\ \beta=+1)$ subset is given in Fig. 5 for $k=20$. This eigenmode is both odd with respect to the origin and the center of the anticyclonic vortices. A dashed line sketches the streamline $\tilde{\psi}=-0.3558$ where the eigenmode should be localized, according to Fig. 4. We can see that the two results agree very well. A detailed comparison of the internal spatial structure of the eigenmode shows that there is a complete accordance between the eigenmode constructed with Bayly's method and the eigenmode obtained by the matrix eigenvalue method. The amplification rate of the eigenmode is $s=0.107$ which has to be compared to the value obtained with Bayly's formalism ($n=0$) for $k=20$: $s=0.1283-0.4913(2\cdot0+1)/20=0.104$.

The precise convergence properties as k increases are investigated in Appendix C 1. There we identify the first 3 members of the family of eigenmodes ($n=0,1,2$) whose amplification rates converge towards a single value as $k\rightarrow\infty$: both the short-wave amplification rate $\sigma(\tilde{\psi})$ and the eigenvalue convergence parameters μ_n are retrieved by the matrix eigenvalue method.

2. Elliptic instabilities

The elliptic instabilities are investigated with $\mathrm{Ro}=7$. The short-wave results were reported in Figs. 2 and 3. The streamline $\tilde{\psi}=+1$ of the cyclonic vortex is unstable with amplification rate $s=0.1387$ and the streamline $\tilde{\psi}=-1$ of the anticyclonic vortex is unstable with amplification rate $s=0.1754$. The short-wave asymptotics shows that the perturbations are not spanwise since the maximum of instability is reached in the center of the vortices for high values of the co-latitude angle θ. Bayly's analysis of Sec. IV A can therefore not be applied and precise convergence properties as $k\rightarrow\infty$ are lacking in this case.

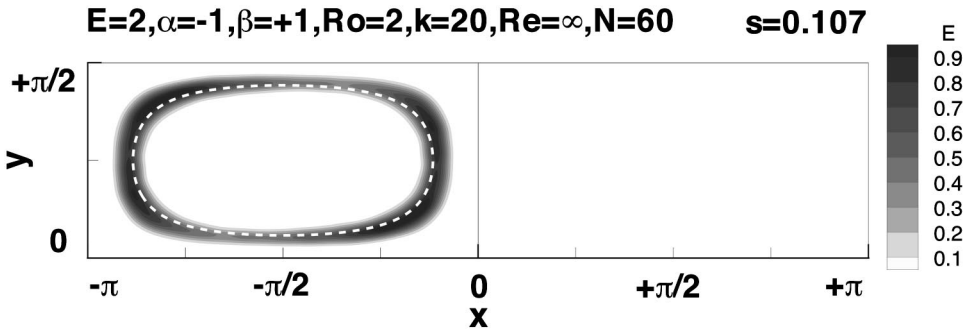

FIG. 5. Energy repartition of a typical centrifugal unstable normal mode obtained by the matrix eigenvalue method. The dashed white line sketches the streamline $\tilde{\psi}=-0.3558$ in the vicinity of which Bayly's method enables us to construct asymptotically the centrifugal unstable normal mode. This mode is odd both with respect to the origin ($\alpha=-1$) and with respect to the center of the anticyclonic vortex $\tilde{\psi}=-1$ ($\alpha\beta=-1$).

The matrix eigenvalue method is conducted with ($\alpha=-1$, $\beta=-1$). The eigenmodes are odd with respect to the origin but are even with respect to the center of the vortices. The spatial resolution is fixed to $-50\leqslant m,n\leqslant 50$ and $\mathrm{Re}=\infty$. In the case $k=10$, Fig. 6 depicts the spatial energy repartition of the most amplified elliptic unstable modes: the upper plot is relative to elliptic instability in the anticyclonic vortex whereas the lower plot concerns the cyclonic case. We can see two eigenmodes which are concentrated in the center of the vortices ($\tilde{\psi}=\pm 1$). Plots of the vertical vorticity perturbation show a dipole structure that is typical of elliptical eigenmodes.[11,13,28] The amplification rates, $s=0.129$ for the cyclonic mode and $s=0.165$ for the anticyclonic mode are close to the values predicted by the short-wave asymptotics.

The convergence properties as $k\to\infty$ are analyzed in Appendix C 2. We show that the structure of the problem is the same as in Sec. IV A: an infinite number of branches ($n=0,1,2,\ldots$) actually converge toward the predicted maximum short-wave amplification rate $\sigma(\tilde{\psi})=\pm 1$ and a single relation for the amplification rates s_n fits all the results: $s_n=\sigma(\tilde{\psi}=\pm 1)-\mu_n/k$ with $\mu_n=(2n+1)\mu_0$ and $\mu_0>0$.

3. Hyperbolic instabilities

The hyperbolic instabilities are investigated for $\mathrm{Ro}=7$. In Sec. III B 3, we established that the hyperbolic stagnation points were unstable, with amplification rate $\sigma(\tilde{\psi}=0,\theta=0)=0.3736$ if $\mathrm{Ro}=7$. Again, Bayly's formalism of Sec. IV A cannot be applied so that a clear link between this short-wave result and a normal mode analysis does not exist. Here, as a result, we could not identify any normal mode whose amplification rate converges toward this last value as k increases. But we have to be very cautious in the interpretation of this result since the explored vertical wavelengths are not that high ($k\leqslant 40$) and the available resolution is quite limited $-60\leqslant m,n\leqslant 60$.

In the case $\mathrm{Ro}=7$ (Fig. 2), we can also see that closed streamlines bear the hyperbolic instability: both the cyclones and the anticyclones undergo instability for streamlines which are close to the bounding streamline $\tilde{\psi}=0$. Here, streamlines with $\sigma'(\psi_0)=0$ and $\sigma''(\psi_0)<0$ do not exist. We can again not apply the results of Sec. IV A, i.e., construct a family of eigenmodes which concentrate along a

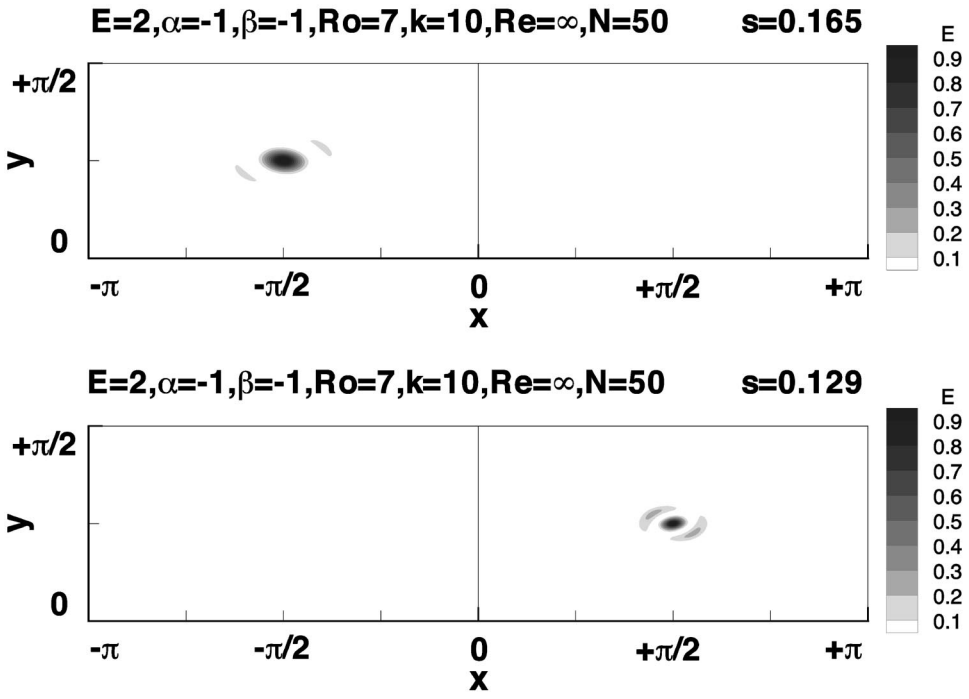

FIG. 6. Energy repartition of two typical elliptic unstable normal modes obtained by the matrix eigenvalue method: the upper plot refers to an anticyclonic mode ($\tilde{\psi}=-1$) whereas the lower plot is a cyclonic mode ($\tilde{\psi}=+1$). These modes are odd ($\alpha=-1$) with respect to the origin but even ($\alpha\beta=+1$) with respect to the center of the vortices $\tilde{\psi}=\pm 1$.

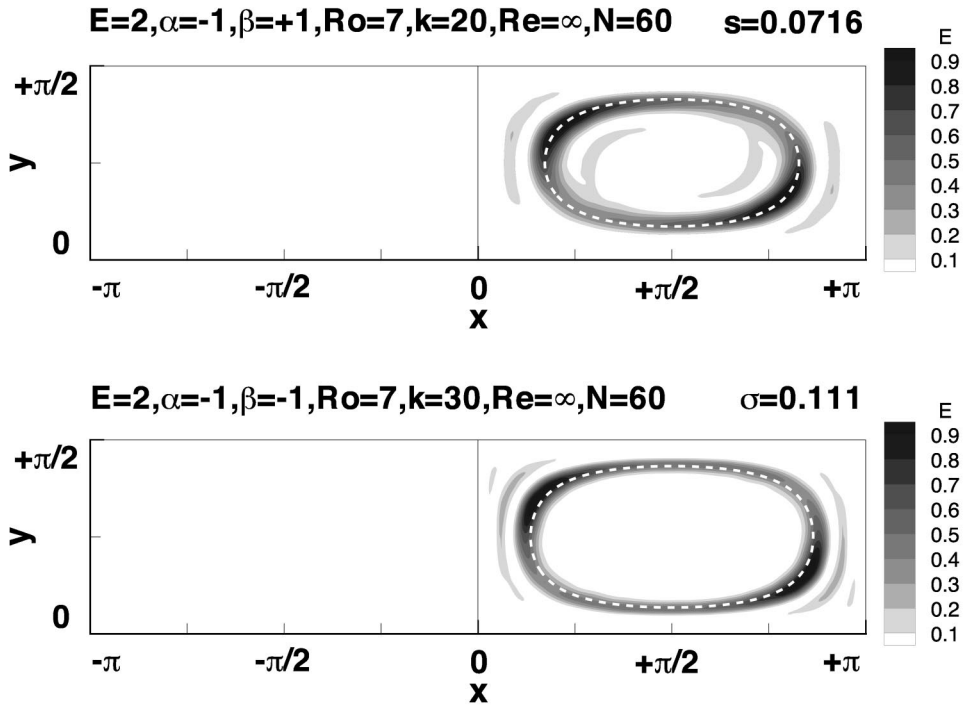

FIG. 7. Energy repartition of a cyclonic unstable normal mode obtained by the matrix eigenvalue method for $k=20$ and $k=30$. It is the same eigenmode but for different k. The dashed white lines sketch the streamlines $\tilde{\psi}=0.515$ (upper plot) and $\tilde{\psi}=0.413$ (lower plot) where the short-wave asymptotics predicts the same amplification rate for spanwise perturbations as the matrix eigenvalue method. These modes are both odd with respect to the origin ($\alpha=-1$) and with respect to the center of the cyclonic vortex $\tilde{\psi}=1$ ($\alpha\beta=-1$).

single ψ_0 and whose amplification rates converge towards $\sigma(\psi_0)$ as $k\to\infty$.

The matrix eigenvalue method is conducted with ($\alpha=-1$, $\beta=+1$) so that the eigenmodes are both odd with respect to the origin and the center of the vortices. The Reynolds number is $\mathrm{Re}=\infty$ and the spatial resolution accounts for $-60\leqslant m,n\leqslant 60$. In the case $k=20$, we identified three cyclonic unstable normal modes which are localized along closed streamlines and whose amplification rates are $\sigma=0.0716$, $\sigma=0.110$ and $\sigma=0.1464$. The first one is represented in the upper plot of Fig. 7. The white dashed line represents the streamline $\tilde{\psi}=0.515$ where the short-wave asymptotics predicts instability (for spanwise perturbations) with the same amplification rate as the one given by the matrix eigenvalue method $\sigma=0.0716$. We can notice that the spatial localization of the eigenmode corresponds approximately to that streamline. The two linear approaches are therefore in accordance. The same conclusions can be drawn from the analysis of the spatial structure of the other two eigenmodes. The only difference is that the eigenmodes are localized along streamlines which are closer to the bounding streamline $\tilde{\psi}=0$. But again, agreement between the two linear approaches is achieved.

As seen in Appendix C 3, here the convergence properties are different from the standard spanwise case of Sec. IV A, where the normal modes concentrate in the neighborhood of a single streamline when k increases. In the present case, we observe that, as k increases, unstable normal modes appear in the center of the vortex near $\tilde{\psi}=0.55$ and then move outward towards $\tilde{\psi}=0$ (see lower plot of Fig. 7). For each value of the wavenumber k, agreement is obtained between the short-wave asymptotics and the normal mode analysis.

V. CONCLUSION

In this article, we have studied the short-wave linear dynamics of the Taylor–Green flow in a rotating system by means of the geometrical optics method and a classical normal mode analysis.

In Sec. III, we have given a complete picture of the short-wave stability properties of the Taylor–Green flow for various Rossby numbers. For high Rossby numbers, it has been shown that cyclones and anticyclones behave similarly and that elliptic instability occurs in the center of the vortices. Hyperbolic instability affects the hyperbolic stagnation points but not the closed streamlines.

When the level of background rotation increases, the cyclones and the anticyclones behave differently. The elliptic instability is first strengthened in the anticyclones, its amplification rate reaching its maximum value for $\mathrm{Ro}=2$. Then the amplification rate decreases and vanishes for $\mathrm{Ro}=1.25$. Below this value, elliptic instability does not affect the anticyclones until $\mathrm{Ro}=0.75$ where it re-emerges again. On the other hand, rotation only weakens elliptic instability in cyclones. We note that for $\mathrm{Ro}=0$, the cyclones and the anticyclones are still unstable with a finite value of the amplification rate.

If $\mathrm{Ro}>1$, an interval of unstable streamlines appears in the center of the anticyclones. This unstable region corresponds to centrifugal instabilities as shown in Ref. 26. As the Rossby number increases, the amplification rate increases and the unstable region moves out towards the bounding streamline $\tilde{\psi}=0$.

Concerning the hyperbolic instability, the amplification rate on the hyperbolic stagnation points decreases as the level of background rotation increases. But in the same time, closed streamlines become affected by this instability both in

the cyclones and in the anticyclones. If Ro$<$2.5, hyperbolic instability vanishes for spanwise perturbations but survives for high co-latitude angles θ.

In Sec. IV A, we have used the short-wave formalism to construct localized normal modes in the vicinity of some streamlines, following Bayly's formalism.[25] This amounts to considering streamlines ψ where the amplification rate $\sigma(\psi)$ of spanwise perturbations (θ=0) is such that: $\sigma'(\psi)=0$ and $\sigma''(\psi)<0$. We have found that localized centrifugal normal modes can be constructed if $1<\mathrm{Ro}<3.2$ and localized elliptic normal modes if Ro$>$3.2.

In Sec. IV B, a matrix eigenvalue method is used in order to compare the results of a direct normal mode analysis with those of the short-wave asymptotics. The centrifugal normal modes in the case Ro=2 have been retrieved and their characteristics (amplification rate and spatial structure) are in accordance with the results of Sec. IV A. The hyperbolically unstable closed streamlines of the cyclones in the case Ro=7 also correspond to localized normal modes whose characteristics agree with the short-wave results. But the convergence properties are not the same as before: as $k\to\infty$, localized eigenmodes emerge in the center of the cyclones around $\tilde{\psi}=0.55$ and move out towards the bounding streamline $\tilde{\psi}=0$. Results of the hyperbolic instability on the stagnation points have not been retrieved: higher vertical wavenumbers should be explored but this requires very high resolution. The short-wave results for elliptic instability in the center of both the cyclones and the anticyclones for the case Ro=7 are in complete agreement with the normal mode analysis: typical elliptic normal modes with amplification rates converging towards the short-wave amplification rates as $k\to\infty$ have been identified.

In brief, from a physical point of view, we have identified the three basic short-wave instabilities that affect rotating vortices. Critical values of the Rossby number Ro have been obtained: for example, the value Ro=1 marks the departure of centrifugal instability in anticyclones, the value Ro=2 corresponds to the maximum value of the amplification rate obtained with elliptic instability in anticyclones. From a technical point of view, we have seen that the short-wave asymptotics and the normal mode analysis are in agreement for centrifugal instability, for elliptic instability occurring in the center of the vortices and for hyperbolic instability developing on closed streamlines. In each case, we have seen that normal modes could be associated to the results given by the short-wave asymptotics.

APPENDIX A: CONSTRUCTION OF NORMAL MODES FOR SPANWISE PERTURBATIONS

In this section, we show how the short-wave asymptotics can be used to construct normal modes in the specific case of spanwise perturbations (θ=0). We follow Bayly's formalism[25] and extend it to the rotating case which is considered here.

Normal modes are sought in the usual way by considering a vertical wavelength k and a complex amplification rate s: $(\mathbf{u}',p')=[\tilde{\mathbf{u}}(x,y),\tilde{p}(x,y)]\exp(ikz+st)$. The main idea is to use a particular vector field basis $\mathbf{f}_i$ for the representation of the eigenmode $\tilde{\mathbf{u}}(x,y)$: $\tilde{\mathbf{u}}(x,y)=\tilde{u}(x,y)\mathbf{f}_1(x,y)+\tilde{v}(x,y)\mathbf{f}_2(x,y)+\tilde{w}(x,y)\mathbf{f}_3(x,y)$. $\mathbf{f}_i(x,y)$ is a vector field which diagonalizes the inertial operator $\mathbf{u}\cdot\nabla(\,)+(\,)\cdot\nabla\mathbf{u}+\mathrm{Ro}^{-1}\mathbf{e}_z\times(\,)$. $\mathbf{f}_i$ is constructed using the eigenvalues $s_i(\psi)$ and the eigenvectors of the fundamental Floquet matrix associated to the differential equation (6) obtained with spanwise perturbations.

In the following, we choose a streamline ψ_0 where the above Floquet exponents $s_i(\psi_0)$ are all real: $s_1(\psi_0)=\sigma(\psi_0)$, $s_2(\psi_0)=-\sigma(\psi_0)$ and $s_3(\psi_0)=0$ where $\sigma(\psi_0)>0$. This means that the inertial operator $\mathbf{u}\cdot\nabla(\,)+(\,)\cdot\nabla\mathbf{u}+\mathrm{Ro}^{-1}\mathbf{e}_z\times(\,)$ has an unstable $\mathbf{f}_1$ direction. We also suppose that $\sigma(\psi)$ takes a quadratic maximum on the streamline ψ_0, i.e., $\sigma'(\psi_0)=0$ and $-\sigma''(\psi_0)>0$.

In the limit $k\to\infty$, the eigenmodes are sought with the following asymptotic behavior in k:

$$\tilde{u}(\eta)=\mathcal{U}(\eta),\quad \tilde{v}(\eta)=k^{-1}\mathcal{V}(\eta),$$
$$\tilde{w}(\eta)=k^{-1/2}\mathcal{W}(\eta)\quad\text{and}\quad \tilde{p}(\eta)=k^{-3/2}\mathcal{P}(\eta), \tag{A1}$$

where $\eta=k^{1/2}(\psi-\psi_0)$ is a re-scaled streamfunction coordinate which enables us to focus in the vicinity of the streamline ψ_0. The dominant part of the eigenvector is therefore along the unstable $\mathbf{f}_1$ direction of the inertial operator $\mathbf{u}\cdot\nabla(\,)+(\,)\cdot\nabla\mathbf{u}+\mathrm{Ro}^{-1}\mathbf{e}_z\times(\,)$.

The scaling of the eigenvalue s is as follows:

$$s=\sigma(\psi_0)-\frac{\mu}{k}, \tag{A2}$$

where μ is a constant to be determined. Hence, as $k\to\infty$, the amplification rate of the constructed eigenmode s converges to the predicted maximum value of the short-wave analysis $\sigma(\psi_0)$. This convergence is achieved with a slope given by the parameter μ, which can be called an eigenvalue convergence parameter.

Introducing this expansion in the linearized Euler equations, we are led to the quantum harmonic oscillator:[23,32]

$$\frac{d^2\mathcal{U}}{d\eta^2}+\left(\frac{\mu}{C(\psi_0)}-\lambda^2\eta^2\right)\mathcal{U}=0,\quad\text{with}\quad \mathcal{U}(\pm\infty)=0, \tag{A3}$$

where

$$\lambda^2=-\frac{\sigma''(\psi_0)}{2C(\psi_0)}, \tag{A4}$$

$$C(\psi_0)=\frac{1}{T(\psi_0)}\int_0^{T(\psi_0)}(\mathbf{f}_1^\dagger\cdot\nabla\psi)\left[\sigma(\psi_0)+\frac{d}{dt}\right](\mathbf{f}_1\cdot\nabla\psi)dt. \tag{A5}$$

In these equations, $\mathbf{f}_i^\dagger(x,y)$ is the adjoint vector field corresponding to $\mathbf{f}_i(x,y)$: $\mathbf{f}_i^\dagger(x,y)\cdot\mathbf{f}_j(x,y)=\delta_{ij}$.

Provided that $-\sigma''(\psi_0)$ and $C(\psi_0)$ are both positive ($\lambda^2>0$), then this equation will have an infinite number of localized eigenfunctions ($n=0,1,2,\ldots$) whose amplification rates $s_n=\sigma(\psi_0)-\mu_n/k$ converge towards $\sigma(\psi_0)$ as $k\to\infty$:

$$\mathcal{U}_n(\eta)=\mathrm{He}_n(\sqrt{2\lambda}\,\eta)\exp\left(-\frac{\lambda\eta^2}{2}\right), \tag{A6}$$

$$\mu_n=(2n+1)\mu_0, \tag{A7}$$

$$\mu_0=\lambda C(\psi_0), \tag{A8}$$

where He_n is the Hermite polynomial of degree n. Hence, for a given wavenumber k, as the branch number n increases, the amplification rate s_n weakens if $\mu_0>0$. In the same time, the complexity of the eigenmode increases in the (x,y) direction. But the eigenmodes remain exponentially concentrated in the neighborhood of the streamline ψ_0 on a characteristic length scale $1/\sqrt{\lambda}$: the parameter λ is therefore a spatial convergence parameter.

APPENDIX B: THE MATRIX EIGENVALUE METHOD

In this appendix, we first present the method of the matrix eigenvalue method. We then analyze the symmetry properties of the flow in order to reduce the linear dynamics into four independent subsets.

1. General equations

The full incompressible viscous Navier–Stokes equations, including the Coriolis force, are linearized around the basic flow. Normal modes will be sought in the form $e^{st}e^{ikz}\phi(x,y)$ where k is the real Oz wavenumber and $s=\sigma+i\omega$ is the complex amplification rate. $\phi(x,y)$ stands for the velocity $(\tilde{u},\tilde{v},\tilde{w})$ and pressure $\tilde{p}$ perturbations and is complex. As the basic flow, the perturbations are assumed to be periodic in the x and y directions, so that $\phi(x,y)=\Sigma_{m,n}\phi(m,n)e^{imx}e^{iEny}$. By eliminating the pressure and the vertical velocity perturbations $\tilde{p}(m,n)$ and $\tilde{w}(m,n)$, we are led to[33]

$$\begin{aligned}s\tilde{u}(m,n)=&\frac{1}{\mathrm{Ro}}\left[\frac{E^2n^2+k^2}{m^2+E^2n^2+k^2}\right]\tilde{v}(m,n)\\&+\left[\frac{1}{\mathrm{Ro}}\frac{Emn}{m^2+E^2n^2+k^2}-\frac{m^2+E^2n^2+k^2}{\mathrm{Re}}\right]\tilde{u}(m,n)\\&+\sum_{m',n'=\pm1}A(m,n,m',n')\tilde{u}(m-m',n-n')\\&+B(m,n,m',n')\tilde{v}(m-m',n-n')\end{aligned} \tag{B1}$$

$$\begin{aligned}s\tilde{v}(m,n)=&-\frac{1}{\mathrm{Ro}}\left[\frac{m^2+k^2}{m^2+\mathrm{E}^2n^2+k^2}\right]\tilde{u}(m,n)\\&+\left[-\frac{1}{\mathrm{Ro}}\frac{Emn}{m^2+E^2n^2+k^2}-\frac{m^2+E^2n^2+k^2}{\mathrm{Re}}\right]\\&\times\tilde{v}(m,n)+\sum_{m',n'=\pm1}C(m,n,m',n')\\&\times\tilde{u}(m-m',n-n')\\&+D(m,n,m',n')\tilde{v}(m-m',n-n'),\end{aligned} \tag{B2}$$

where

$$A(m,n,m',n')=-\frac{E}{4(1+E^2)}\left[1+mm'-nn'+2\frac{mm'nn'-m^2}{m^2+E^2n^2+k^2}\right], \tag{B3}$$

$$B(m,n,m',n')=-\frac{E^2}{4(1+E^2)}\times\left[m'n'+2\frac{mn-m^2m'n'}{m^2+E^2n^2+k^2}\right], \tag{B4}$$

$$C(m,n,m',n')=+\frac{1}{4(1+E^2)}\times\left[m'n'+2E^2\frac{mn-n^2m'n'}{m^2+E^2n^2+k^2}\right], \tag{B5}$$

$$D(m,n,m',n')=+\frac{E}{4(1+E^2)}\left[1-mm'+nn'+2E^2\frac{mm'nn'-n^2}{m^2+E^2n^2+k^2}\right]. \tag{B6}$$

The definition of the Reynolds and Rossby numbers has already been given and we recall that we took $L=a$ and $T=1/W$ as the unit length and time scales.

The procedure is then as follows. We represent this linear operator with a matrix, in which each component corresponds to a mode interaction. We truncate this matrix by representing only a finite number of modes $-N\leqslant m,n\leqslant N$. We finally solve numerically the eigenvalue/eigenvector problem by means of a standard QR algorithm.

2. Symmetries of the flow

In this section, we will prove that the eigenmodes can be decomposed into 4 independent subsets. These will be referred by 2 parameters α and β, each of which can be set to -1 or $+1$. The meaning of each parameter will be clarified below.

First, the problem is invariant under the transformation $x\to-x$, $y\to-y$ and $z\to z$. An eigenvector $(\tilde{u}(m,n),\tilde{v}(m,n))$ therefore necessarily bears the following symmetries:

$$\tilde{u}(-m,-n)=\alpha\tilde{u}(m,n)\quad\text{and}\quad\tilde{v}(-m,-n)=\alpha\tilde{v}(m,n), \tag{B7}$$

where $\alpha=\pm1$.

Secondly, as pointed out by Bayly,[27] the eigenmodes can be decomposed into two independent subsets: the even modes where $m+n$ is even and the odd modes where $m+n$ is odd. This comes from the fact that each mode (m,n) is only coupled with the four neighboring modes $(m-1,n-1)$, $(m-1,n+1)$, $(m+1,n-1)$, $(m+1,n+1)$. The parameter dedicated to this parity is $\beta=(-1)^{m+n}$.

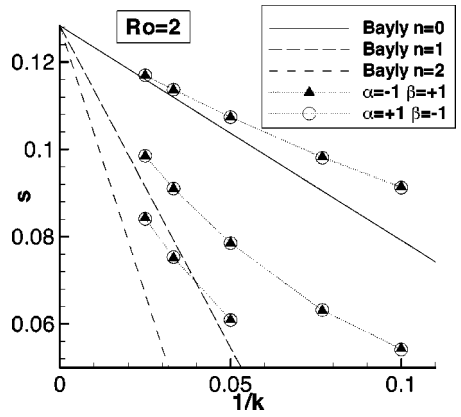

FIG. 8. A comparison between the results given by the short-wave asymptotics (lines) and those given by a matrix eigenvalue method (symbols) for the centrifugal instability in the case Ro=2. The solid, long-dashed and dashed lines represent the first 3 ($n=0,1,2$) asymptotic relations $s_n=0.1283-0.4913(2n+1)/k$. These amplification rates are associated to eigenmodes which are more and more localized in the vicinity of the streamline $\tilde{\psi}=-0.3558$ as $k\to\infty$. The matrix eigenvalue results, i.e., the filled triangles and the empty circles, converge towards these first order asymptotic results.

These symmetries in the spectral space correspond to symmetries in the physical space. If $\phi(x,y)$ stands for the velocity perturbations $\tilde{u}(x,y)$ or $\tilde{v}(x,y)$, then it can be verified that

(i) $\phi(-x,-y)=\alpha\phi(x,y)$ which means that the eigenmode is even ($\alpha=+1$) or odd ($\alpha=-1$) with respect to the origin;

(ii) if $x_1+x_2=\pm\pi$ and $y_1+y_2=\pm\pi/E$ then $\phi(x_2,y_2)=\alpha\beta\phi(x_1,y_1)$. The eigenmode is even ($\alpha\beta=+1$) or odd ($\alpha\beta=-1$) with respect to the center of each vortex ($x=\pm\pi/2, y=\pm\pi/2E$).

APPENDIX C: CONVERGENCE PROPERTIES AS *k* INCREASES

1. Centrifugal instabilities

Centrifugal instabilities are investigated in the particular case Ro=2. As indicated in Sec. IV A, the centrifugal eigenmodes are odd with respect to the center of the anticyclonic vortex ($\tilde{\psi}=-1$). This is why the matrix eigenvalue method is led with $\alpha\beta=-1$: the eigenmodes ($\alpha=-1$, $\beta=+1$) are both odd with respect to the origin and the center of the vortices; the eigenmodes ($\alpha=+1$, $\beta=-1$) are even with respect to the origin but odd with respect to the center of the vortices. Figure 8 sketches the amplification rates s of some particular nonoscillating instabilities versus the inverse of the wavenumber k. The symbols (filled triangles and empty circles) refer to the results obtained by the matrix eigenvalue method and the solid, long-dashed and dashed lines refer to the first 3 ($n=0,1,2$) eigenmodes obtained in Sec. IV A, whose amplification rates converge towards $\sigma(\tilde{\psi})$ as $k\to\infty$: $s_n=\sigma(\tilde{\psi})-\mu_n/k$.

It has first to be noticed that the filled triangles and the empty circles coincide. In fact, the two corresponding eigenvectors have exactly the same structure except that the first one is odd with respect to the origin and the second one is even. Now, since the normal modes are concentrated in the anticyclonic vortices, by linear superposition, one is able to localize the eigenmode either in the cell ($-\pi<x<0, 0<y<\pi/E$) or in the cell ($0<x<\pi, -\pi/E<y<0$). This is important since a localized instability on one vortex is independent of the dynamics of the other vortices.

The amplification rates of the 3 eigenmodes that we are following converge towards the corresponding asymptotic relations of Sec. IV A as $k\to\infty$. The discrepancy that we observe for finite k comes from the fact that the asymptotic relations for s_n are only first order in $1/k$. As suggested by Bayly,[25] one could refine the asymptotic analysis to higher orders: $s_n=\sigma(\tilde{\psi})+\mu_n^{(1)}/k+\mu_n^{(2)}/k^2+\cdots$ Hence, 2nd order corrections could be found which would explain this discrepancy. But the overall results are very good: for the first three eigenmodes, both the slope and the extrapolated asymptotic amplification rate for $k=\infty$ are retrieved.

2. Elliptic instabilities

The elliptic instabilities are investigated with Ro=7. All these eigenmodes are even with respect to the center of the vortices. This is why the matrix eigenvalue methods are led with $\alpha\beta=+1$. Furthermore, all the results that will be shown below are relative to the set of parameters $\alpha=-1$, $\beta=-1$. It

TABLE I. Comparison between amplification rates of elliptic eigenmodes given by the matrix eigenvalue method (columns 2–5) and the maximum amplification rate over θ given by the short-wave asymptotics in the center of the vortices $\tilde{\psi}=\pm1$ (column 6). Column 7 estimates the discrepancy between the two linear methods. Case $E=2$, Ro=7, Re=∞, $\alpha=-1$, $\beta=-1$, $N=50$.

Localization/ Branch number	Normal modes $\sigma(k=10)$	$\sigma(k=20)$	$\sigma(k=\infty)$[a]	Slope[b]	Lifschitz and Hameiri $\sigma(\tilde{\psi}=\pm1)$	Discrepancy %
Cyclonic 0	0.1293	0.1340	0.1387	0.094	0.1387	0
Cyclonic 1	0.1105	0.1246	0.1387	0.282	0.1387	0
Cyclonic 2	0.0917	0.1153	0.1389	0.472	0.1387	0.2
Cyclonic 3	0.0723	0.1059	0.1395	0.672	0.1387	0.5
Anticyclonic 0	0.1647	0.1700	0.1753	0.106	0.1755	0.1
Anticyclonic 1	0.1446	0.1595	0.1744	0.298	0.1755	0.6
Anticyclonic 2	0.1244	0.1493	0.1742	0.498	0.1755	0.7

[a]σ_0 as extrapolated from the results of $k=10$ and $k=20$ assuming a relation of the form $\sigma=\sigma_0-\mu/k$.
[b]μ as extrapolated from the results of $k=10$ and $k=20$ assuming a relation of the form $\sigma=\sigma_0-\mu/k$.

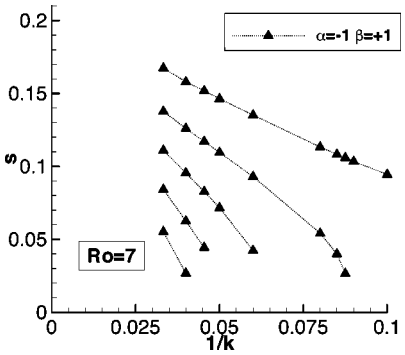

FIG. 9. Amplification rates of unstable cyclonic normal modes localized in the vicinity of closed streamlines in the case Ro=7 as given by the matrix eigenvalue method. As k increases, new unstable eigenmodes appear in the center of the cyclones and move outward towards $\tilde{\psi}=0$.

can be verified that in each case a calculation with $\alpha=+1$, $\beta=+1$ gives approximately the same eigenvalues, so that one can construct localized eigenmodes on only one vortex.

We have sketched in Table I the amplification rates σ of various elliptical modes (4 cyclonic modes and 3 anticyclonic modes) for $k=10$ and $k=20$ (columns 2 and 3). An extrapolated value σ_0 for $k=\infty$ has been calculated (column 4) using the results obtained for $k=10$ and $k=20$ and assuming a relation of the type $\sigma=\sigma_0-\mu/k$. The eigenvalue convergence parameter μ has also been evaluated in each case (column 5). The sixth column indicates the maximum value of the amplification rate $\sigma(\tilde{\psi})$ obtained in the center of the corresponding (cyclonic and anticyclonic) vortex by the short-wave asymptotics and the last column evaluates the discrepancy in percentages between σ_0 and $\sigma(\tilde{\psi})$. This discrepancy is very small ($<1\%$) so that a first order model of the form $\sigma=\sigma_0-\mu/k$ with $\sigma_0=\sigma(\tilde{\psi})$ is very efficient. Besides, by comparing the various slopes μ, we can show that all branches of the cyclonic instabilities are well represented by $s_n=0.1387-0.094(2n+1)/k$. Also, all branches of the anticyclonic instabilities are represented by a unique formula: $s_n=0.1755-0.106(2n+1)/k$. The structure of the solutions is therefore exactly the same as the structure obtained with Bayly's formalism for spanwise perturbations.

3. Hyperbolic instabilities

Hyperbolic instabilities on closed streamlines are investigated with Ro=7. These normal modes should be odd with respect to the center of the vortices $\tilde{\psi}=\pm 1$ so that the calculations are led with $\alpha\beta=-1$. In the case $k=20$, $\alpha=-1$, $\beta=+1$ with $-60\leqslant m,n\leqslant 60$, we identified in Sec. IV B 3 a cyclonic unstable normal mode which is localized along a closed streamline and whose amplification rate is $\sigma=0.0716$. Let us follow this eigenmode when we increase k. If $k=30$, the amplification rate becomes $\sigma=0.111$ and the lower plot of Fig. 7 represents the spatial energy repartition of the corresponding eigenmode. The dashed white line represents the streamline $\tilde{\psi}=0.413$ where the short-wave asymptotics predicts the same amplification rate $\sigma=0.111$ as the matrix eigenvalue method. The spatial localization of the eigenmode again agrees with this streamline. Comparing the case $k=20$ and $k=30$, we easily notice that the localizing streamline ($\tilde{\psi}=0.515$ for $k=20$ and $\tilde{\psi}=0.413$ for $k=30$) is moving outward towards the bounding streamline $\tilde{\psi}=0$. This phenomenon is actually observed for all eigenmodes which are localized on closed cyclonic streamlines.

In brief, for a given vertical wavenumber k, a whole family of localized eigenmodes in the neighborhood of closed streamlines do exist. The amplification rate of each eigenmode is in accordance with the results of the short-wave asymptotics. As k increases, the eigenmodes move outward towards $\tilde{\psi}=0$ while their amplification rates increase. At the same time, new unstable eigenmodes appear in the central part of the vortex near $\tilde{\psi}=0.55$ and begin moving outward. The emergence of new unstable eigenmodes can be seen in Fig. 9 where the amplification rates of some cyclonic normal modes which are concentrated in the neighborhood of closed streamlines have been sketched versus the inverse of the wavenumber k.

[1] E. J. Hopfinger, F. K. Browand, and Y. Gagne, ''Turbulence and waves in a rotating tank,'' J. Fluid Mech. **125**, 505 (1982).
[2] R. C. Kloosterziel and G. J. F. van Heijst, ''An experimental study of unstable barotropic vortices in a rotating fluid,'' J. Fluid Mech. **223**, 1 (1991).
[3] I. Mutabazi, C. Normand, and J. E. Wesfreid, ''Gap size effects on centrifugally and rotationally driven instabilities,'' Phys. Fluids A **4**, 1199 (1992).
[4] G. F. Carnevale, M. Briscolini, R. C. Kloosterziel, and G. K. Vallis, ''Three-dimensionally perturbed vortex tubes in a rotating flow,'' J. Fluid Mech. **341**, 127 (1997).
[5] P. G. Drazin and W. H. Reid, *Hydrodynamic Stability* (Cambridge University Press, Cambridge, 1981).
[6] R. C. Kloosterziel and G. F. Carnevale, ''Formal stability of circular vortices,'' J. Fluid Mech. **242**, 249 (1992).
[7] P. Orlandi and G. F. Carnevale, ''Evolution of isolated vortices in a rotating fluid of finite depth,'' J. Fluid Mech. **381**, 239 (1999).
[8] K. S. Eckhoff, ''On stability for symmetric hyperbolic systems I,'' J. Diff. Eqns. **40**, 94 (1981).
[9] A. Lifschitz and E. Hameiri, ''Local stability conditions in fluid dynamics,'' Phys. Fluids A **3**, 2644 (1991).
[10] R. T. Pierrehumbert, ''Universal short-wave instability of two-dimensional eddies in an inviscid fluid,'' Phys. Rev. Lett. **57**, 2157 (1986).
[11] B. J. Bayly, ''Three-dimensional instability of elliptical flow,'' Phys. Rev. Lett. **57**, 2160 (1986).
[12] M. J. Landman and P. G. Saffman, ''The three-dimensional instability of strained vortices in a viscous fluid,'' Phys. Fluids **30**, 2339 (1987).
[13] F. Waleffe, ''On the three-dimensional instability of strained vortices,'' Phys. Fluids A **2**, 76 (1990).
[14] G. K. Batchelor and I. Proudman, ''The effect of rapid distorsion on a fluid in turbulent motion,'' Q. J. Mech. Appl. Math. **7**, 83 (1954).
[15] R. R. Lagnado, N. Phan-Thien, and L. G. Leal, ''The stability of two-dimensional linear flows,'' Phys. Fluids **27**, 1094 (1984).
[16] A. D. D. Craik and W. O. Criminale, ''Evolution of wavelike disturbances in shear flows: a class of exact solutions of the Navier-Stokes equations,'' Proc. R. Soc. London, Ser. A **406**, 13 (1986).
[17] S. Friedlander and M. M. Vishik, ''Instability criteria for the flow of an inviscid incompressible fluid,'' Phys. Rev. Lett. **66**, 2204 (1991).
[18] S. Leblanc and F. S. Godeferd, ''An illustration of the link between ribs and hyperbolic instability,'' Phys. Fluids **11**, 497 (1998).
[19] A. D. D. Craik, ''The stability of unbounded two- and three-dimensional flows subject to body forces: some exact solutions,'' J. Fluid Mech. **198**, 275 (1989).
[20] C. Cambon, J.-P. Benoit, L. Shao, and L. Jacquin, ''Stability analysis and large eddy simulation of rotating turbulence with organized eddies,'' J. Fluid Mech. **278**, 175 (1994).
[21] B. J. Bayly, D. D. Holm, and A. Lifschitz, ''Three-dimensional stability of elliptical vortex columns in external strain flows,'' Philos. Trans. R. Soc. London, Ser. A **354**, 895 (1996).

[22]S. Leblanc and F. S. Godeferd, ''Coherence of vortices in a rotating fluid,'' *Proceedings of the Eleventh Symposium on Turbulent Shear Flows*, Grenoble, France, 1997.
[23]S. Leblanc and C. Cambon, ''On the three-dimensional instabilities of plane flows subjected to Coriolis force,'' Phys. Fluids **9**, 1307 (1997).
[24]S. Leblanc, ''Stability of stagnation points in rotating flows,'' Phys. Fluids **9**, 3566 (1997).
[25]B. J. Bayly, ''Three-dimensional centrifugal-type instabilities in inviscid two-dimensional flows,'' Phys. Fluids **31**, 56 (1988).
[26]D. Sipp and L. Jacquin, ''Three-dimensional centrifugal-type instabilities of two-dimensional flows in rotating systems,'' submitted to Phys. Fluids.
[27]B. J. Bayly, ''Computations of broad-band instabilities in a class of closed-streamline flows,'' in *Mathematical Aspects of Vortex Dynamics,* edited by R. E. Caflisch (SIAM, Philadelphia, 1989), pp. 50–58.
[28]D. Sipp and L. Jacquin, ''Elliptic instability in two-dimensional flattened Taylor-Green vortices,'' Phys. Fluids **10**, 839 (1998).
[29]A. Lifschitz, ''Essential spectrum and local stability condition in hydrodynamics,'' Phys. Lett. A **152**, 199 (1991).
[30]M. Vishik and S. Friedlander, ''Dynamo theory methods for hydrodynamic stability,'' J. Math. Pures Appl. **72**, 145 (1993).
[31]C. Cambon and F. S. Godeferd, ''Stability of Stuart's vortices in a rotating frame,'' in preparation, to be submitted to Phys. Fluids.
[32]C. M. Bender and S. A. Orszag, *Advanced Mathematical Methods For Scientists and Engineers* (McGraw-Hill, New York, 1978).
[33]E. Lauga, ''Stabilité des tourbillons de Taylor-Green en rotation,'' Stage d'Option Scientifique, Ecole Polytechnique, 1998.